MRS Communications (2018), *8*, 15–28

doi:10.1557/mrc.2018.19

MRS Communications

Prospective Article

Temperature-dependent nanoindentation response of materials

Saeed Zare Chavoshi, Department of Mechanical Engineering, Imperial College London, London SW7 2AZ, UK
Shuozhi Xu, California NanoSystems Institute, University of California, Santa Barbara, Santa Barbara, CA 93106-6105, USA
Address all correspondence to Saeed Zare Chavoshi at **s.zare@imperial.ac.uk**

(Received 11 December 2017; accepted 6 February 2018)

Abstract

It is of the uttermost interest to understand the mechanical performance and deformation mechanisms contributing to small-scale plasticity of materials in micro/nanoelectromechanical systems at their service temperatures, which are usually above room temperature. In recent years, high-temperature nanoindentation experiments have emerged as a reliable approach to characterize the deformation behavior of materials at the nano and submicron scale. In this review, we highlight the role of the temperature in nanoindentation response of a wide variety of materials, with a particular focus on the thermally-activated deformation mechanisms in crystalline and non-crystalline materials under the indenter, e.g., dislocation processes, shear transformation zone, and phase transformations. A brief survey of the temperature-dependent nanoindentation elastic modulus, hardness, and creep behavior of materials is also provided. We also discuss experimental methods for correctly measuring the mechanical properties of materials at high temperatures.

Introduction

The focus of scientific research within the past decade has shifted to the investigation of the material behavior at the nanoscale. The proliferation of researchers studying materials on this length scale has resulted in the invention of the phrase "nanotechnology". Meanwhile, studies of mechanical properties on this scale have led to the term "nanomechanics", which is a subfield of mechanics characterizing the mechanical behavior of materials at atomic level subject to different types of boundary conditions.[1] As almost all mechanical properties of materials are temperature-dependent, small-scale characterization at high temperatures could lead to substantial opportunities in nanomechanics to understand material behavior at service temperatures and conditions relevant to industrial applications.[2] Accordingly, high-temperature nanomechanical testing techniques, predominantly high-temperature nanoindentation, are becoming increasingly popular among researchers within the nanomechanics community. The simplicity of the sample requirement, automated data collection and analysis, as well as the capability to probe small-scale physical phenomena in materials, such as dislocation nucleation, shear band activation, and phase transformations, have made high-temperature nanoindentation a powerful tool for small-scale materials characterization at elevated temperatures.[3] On the other hand, regardless of the specimen size, reliable high-temperature characterization calls for precise application and measurement of deformation (load or displacement) while concurrently controlling and measuring sample temperatures. Fundamentally, instrumented high-temperature nanoindentation requires additional instrumentation advances in two fields: (i) minimizing or eliminating oxidation and (ii) successful management of thermal drift and noise.[4,5] Procedures for satisfying these requirements have been discussed in the literature. These include works by Wheeler and co-workers[3,6,7] and those brought forward by Schuh and his colleagues.[5,8–10] For the sake of brevity, they are not elaborated in this paper and interested readers are referred to relevant publications to comprehend the high-temperature nanoindentation instrumentations.

In this review, we systematically describe the influence of temperature on the mechanical behavior and corresponding plasticity mechanisms involved in nanoscale deformation of various materials subject to high-temperature nanoindentation loading. Our review provides an in-depth understanding of the mechanisms of surface plasticity at high temperatures where the interactions between thermal activation processes and surface stresses multiply the defect formation and nanoscale effects accompanied by the macroscopic mechanisms. In the remainder of this paper, thermally-activated deformation mechanisms in crystalline and non-crystalline materials under indenter, e.g., dislocation processes, shear transformation zone (STZ), and phase transformations, are elaborated; then the way to correctly measure mechanical properties of materials at high temperatures is explained and mechanical response of materials at elevated temperatures is discussed; research challenges and future directions in the field of high temperature nanoindentation are outlined in the last section of the paper.

Nanoscale deformation mechanisms

Heat content plays a crucial role in the deformation of microstructures and onset of nanoscale plasticity. As shown in

Fig. 1, an increase in temperature leads to increased activities of phonons (in crystalline insulators and some semi-conductors), electrons (in metal and some semi-conductors), propagons, diffusons, and locons (in amorphous non-metallic materials),[11,12] which in turn contribute to additional atomic displacements, an increase in the average interatomic distance, and a decrease in the restoring forces due to thermal expansion.[13–16] While increasing the dislocation mobility, a higher temperature lowers the minimum stresses required for homogeneous dislocation nucleation, dislocation gliding in a lattice, and breaking dislocation locks. As a result, thermal softening improves the plasticity of the material.[17,18]

In the following, we focus on the insights provided by the high-temperature nanoindentation into the thermally-activated processes, activation energies, volumes, and the onset of plasticity. First, the plasticity of crystalline materials, primarily the thermally-activated dislocation processes, is discussed. Plasticity of non-crystalline materials is then covered, where the STZ mechanisms beneath the indenter at high temperatures are elaborated. Finally, a section is devoted to the phase transformation during nanoindentation at elevated temperatures.

Plasticity of crystalline materials

Thermally-activated dislocation plasticity in crystalline materials can be examined by high temperature nanoindentation experiments. Dark-field transmission electron microscopy (TEM) images of $Mg_{17}Al_{12}$ underneath the indentation shown in Fig. 2 indicate that at room temperature, dislocations are straight and mostly gliding on particular parallel slip planes extending to the surface with increasing dislocation entanglement towards the center of the plastic zone. At high temperatures, e.g., 278 °C, more homogeneous dislocation distribution is achieved, exhibiting a curved shape with some dissociation.[19]

Nanoindentation tests of the two-phase eutectic Sn-Bi alloy up to 100 °C reveal that the dislocation climb controlled by core diffusion and power-law breakdown, in which the deformation is governed by dislocation glide-controlled flow, are the dominant creep and deformation mechanisms, respectively.[20] Dislocation climb motion controlled by the dislocation pipe mechanism is reported to be the creep mechanism of the bulks of low-Ag Cu/Sn-Ag-Cu-Bi-Ni/Cu microsolder joints up to 85 °C.[21]

The occurrence of "pop-in" events in nanoindentation, i.e., sudden depth excursions under load control or sudden load drops under displacement control, is associated with the dislocation activity. As illustrated in Fig. 3(a), at room temperature, one large discontinuity is observed on the load-displacement (*P-h*) curves, whereas at 200 °C, multiple pop-ins separated by elastic reloading segments occur, resulting in a highly serrated *P-h* curve.[22,23] The serrated flow behavior is a result of the defect evolution owing to the special quasi-elastic reloading. On the other hand, thermally-activated deformation processes, e.g., dislocation nucleation or abrupt release of dislocation entanglements causes the appearance of multiple pop-ins and discontinuity. Note that the Taylor dislocation model[24] can be adopted to determine the temperature effects on the friction stress of screw dislocations.[25–27] Taylor dislocation model relates the shear flow stress to the dislocation density. It is also widely used to describe the indentation size effect (ISE). As shown in Fig. 3(b), the friction stress and friction coefficient decrease with increasing temperature, which is in agreement with the mobilization of screw dislocations at the critical temperature, $T_c = 177$ °C, where screw dislocations become mobile.[22]

As seen in Figs. 4(a) and 4(b), indentation of pure Pt at high temperatures leads to the discretization of plasticity into sharp bursts of activity. Based on the complementary mathematical

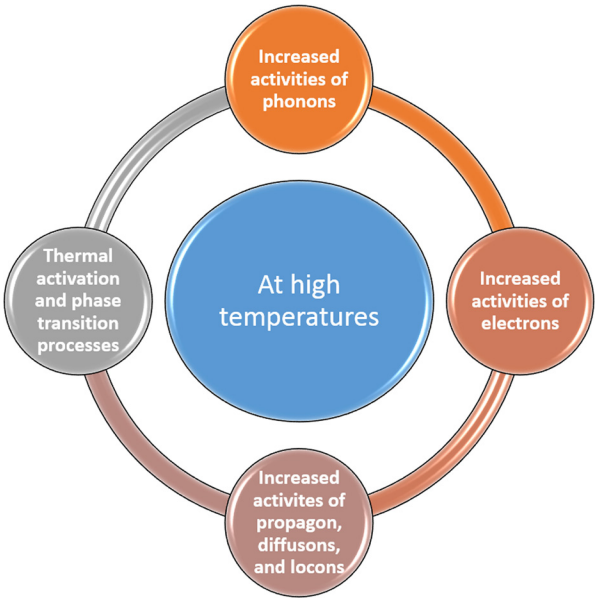

Figure 1. Temperature-dependent phenomena in materials during high-temperature nanoindentation.

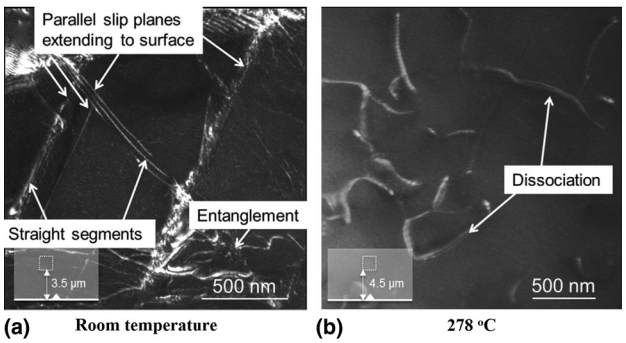

Figure 2. Dark-field TEM of the indentation imprint on $Mg_{17}Al_{12}$. More homogeneous dislocation distribution exhibiting a curved shape with some dissociation is seen at the high temperature. Adopted with permission from Ref.[19] (Elsevier, 2016).

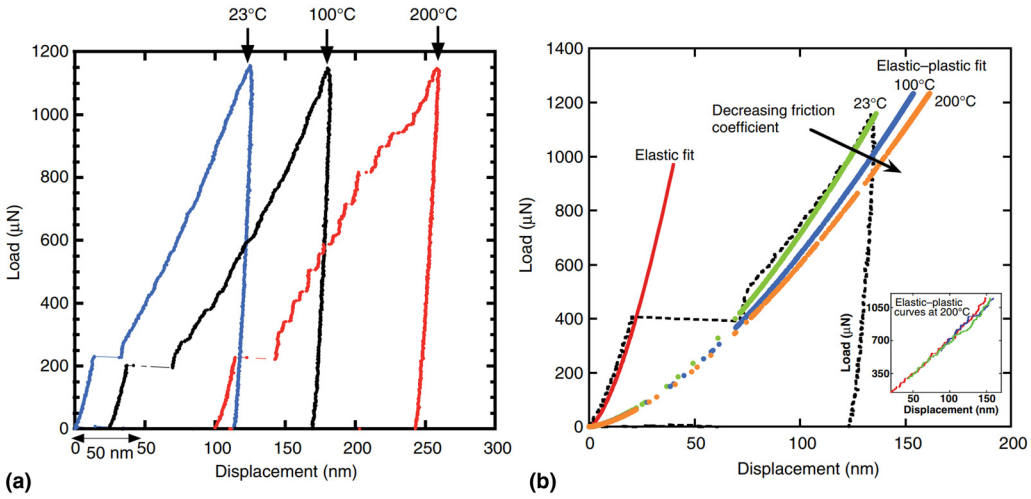

Figure 3. (a) *P-h* curves from the nanoindentation of Ta at a loading rate of 1000 μN/s at different temperatures, (b) Elastic-plastic and elastic fit; the dashed curve is from experiments at 23 °C. Friction coefficient decreases with temperature. Adopted with permission from Ref.[22] (Taylor & Francis, 2010).

approaches,[28,29] the onset of plasticity of Pt is explained by heterogeneous process of dislocation nucleation, with an atomic-scale, low-energy event as the rate limiter.[30] An analysis based on the total activation energy and activation volume indicates that screw dislocation cross-slip governs the operative plastic deformation of Mg, regardless of the strain rate and temperature (<300 °C).[31] Nanoindentation experiments of high-purity Cr have also revealed the existence of thermally-activated strength component superimposed on a temperature-/rate-independent strength contribution, attributable to the propagation of screw dislocations governed by thermally-activated kink-pair nucleation.[32] Similarly, indentation plastic deformation of ultrafine-grained (UFG) Cu-Nb composite with a randomly distributed oriented grain size ~100–200 nm up to 300 °C is controlled by dislocation glide and nucleation of kink pairs. However, the plasticity mechanism changes to thermally-activated processes at grain boundaries (GBs) at higher temperatures.[33] As for the UFG Al with a grain size of ~400 nm, when the temperature increases, the type of dislocation interaction with GBs changes from dislocation motion along GBs to dislocations emitted from GBs into the lattice and finally, at the highest temperatures, to diffusion of Al along the GBs. The onset of diffusion-based deformation is observed at lower temperatures for UFG Al than for conventional grained (CG) Al with grain size of ~80 μm, which is consistent with that the GB activity increases with decreasing grain size. Creep behavior during the indentation strain rate jumps, where several abrupt changes in the applied strain rate at

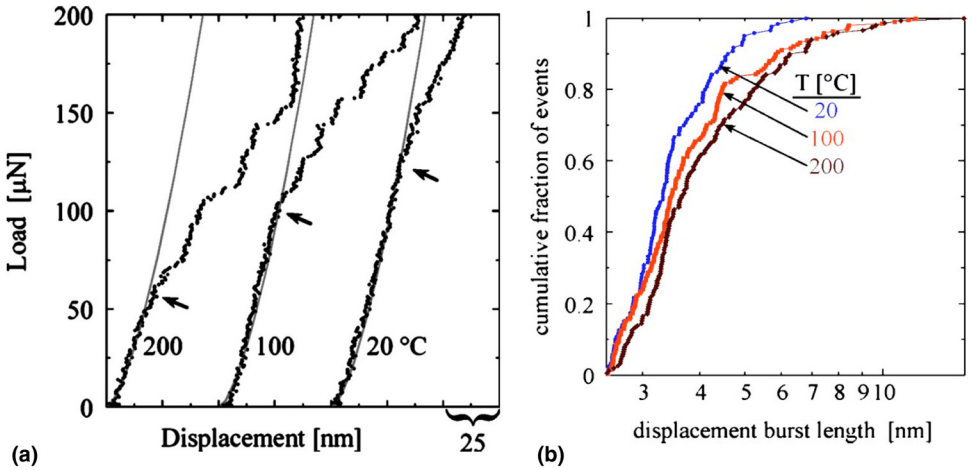

Figure 4. (a) *P-h* curves from the nanoindentation of Pt (100) at different temperatures, (b) cumulative fraction of pop-in events. Displacement bursts increase with temperature. Adopted with permission from Ref.[28] (American Institute of Physics, 2004).

defined indentation depths during one single indentation are used,[34] is thought to have masked any change in the activation volume at elevated temperatures.[35]

Plasticity of non-crystalline materials

Bulk metallic glasses (BMGs) have recently attracted much interest, primarily due to their exclusive combination of mechanical and functional properties. One of the most momentous thermophysical properties of BMGs is the glass transition temperature (T_g), higher than which a transition from a hard and relatively brittle glassy state into a viscous or rubbery state occurs. If a BMG is heated to a considerable fraction of its T_g, ~0.75 T_g or higher, its strength decreases significantly as a result of delocalization of deformation as well as homogeneous occurrence of diffuse strain accommodation throughout the stressed material. High temperature nanoindentation studies in $Au_{49}Ag_{5.5}Pd_{2.3}Cu_{26.9}Si_{16.3}$ BMG show that inhomogeneous-to-homogeneous flow transition and reverse ISE occurs when the temperature approaches $T_g = 130$ °C,[36,37] which can be explained in terms of the free volume theory.[36] Notice that the free volume model[38–40] can be adopted to calculate the volume of a basic shear flow unit STZ and the thermal activation energy of a metallic glass.

Amorphous $Pd_{40}Ni_{40}P_{20}$ and $Mg_{65}Cu_{25}Gd_{10}$ metallic glasses have demonstrated two different regimes of homogeneous flow under nanoindentation loading: the first one correlates with the onset of viscous deformation at high temperatures and low rates; the second one corresponds to the high rates at temperatures well below the glass transition, and arises when the deformation rate exceeds the characteristic rate for shear band nucleation, kinetically forcing strain distribution.[41]

Figure 5 compares a time-series of topographical images of single indentations implemented at 176 and 250 °C on $Pt_{57.5}Cu_{14.7}Ni_{5.3}P_{22.5}$ metallic glass, where the viscous-plastic shape recovery at high temperatures is observed due to the surface-tension-driven viscous flow.[42] Such surface tension of metallic glasses in the supercooled liquid temperature range can be modeled by an elastic-viscoplastic constitutive theory developed by Henann and Anand.[43] Self-smoothing of metallic glass surfaces[44] is also witnessed at temperatures above T_g.[42]

As seen in Fig. 6(a), for similar levels of penetration depth, the high-temperature indentations in Zr-based BMG demonstrate considerably fewer numbers of shear offset displacements than at room temperatures. Also, the onset of shear offsets transpires at higher depths of penetration, culminating in a lower total pile-up at the edge of the indentation. Temperature also affects the morphology of the shear offsets, i.e., at room temperature a pointed apex is seen while at 200 °C, a smooth semicircular aspect is realized. *P-h* curves presented in Fig. 6(b) indicate the increase of serrated flow with temperature.[45,46] Fig. 6(c) demonstrates that hardness of Zr-based BMG increases linearly with temperature from an average of 7 GPa at 25 °C to 7.6 GPa at 200 °C, while the reduced Young's modulus marginally decreases from 105 GPa to 103 GPa.

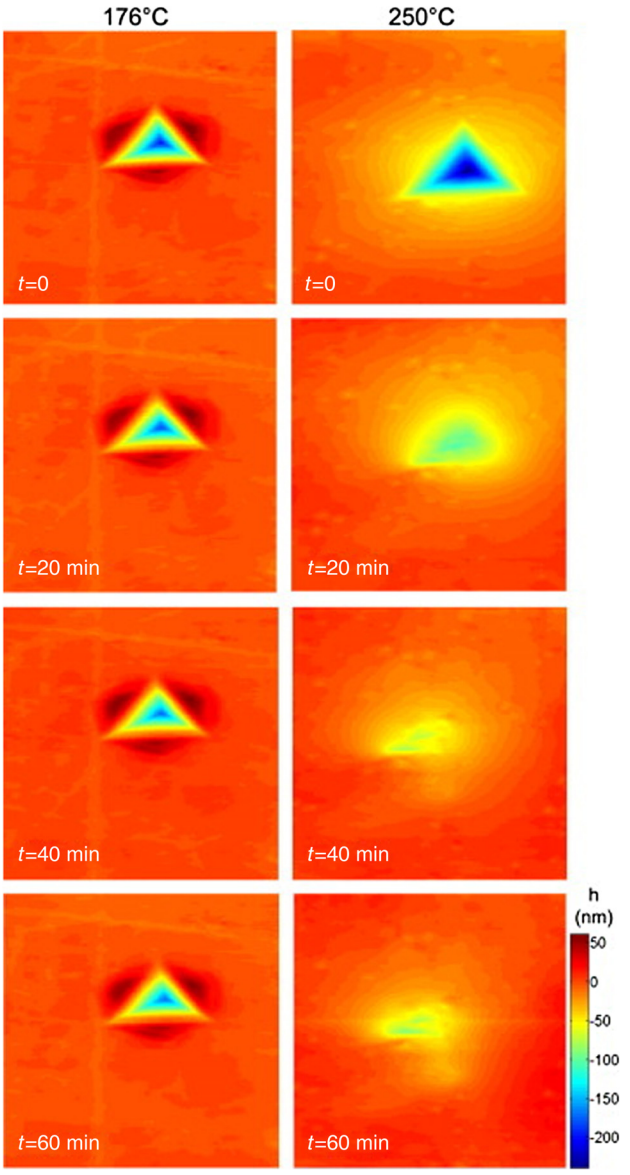

Figure 5. Topographic images of two indentations in Pt-based metallic glass at 176 and 250 °C after unloading, illustrating relative stability and substantial shape recovery, respectively. *h* in the legend indicates the surface roughness. Adopted with permission from Ref.[42] (Elsevier, 2009).

The increase of hardness with temperature is explained by the increase of friction and energy consumed by the progressively thermally favored formation/reactivation of shear band deformation, which is prevented from contributing to a total penetration depth in the form of pop-ins during the displacement-controlled indentation.[45]

Phase transformation

Indentation with a nanoscale tip is known to induce a phase transformation in Si at room temperature. Minomura and Drickamer[47] were the first to discover the change of

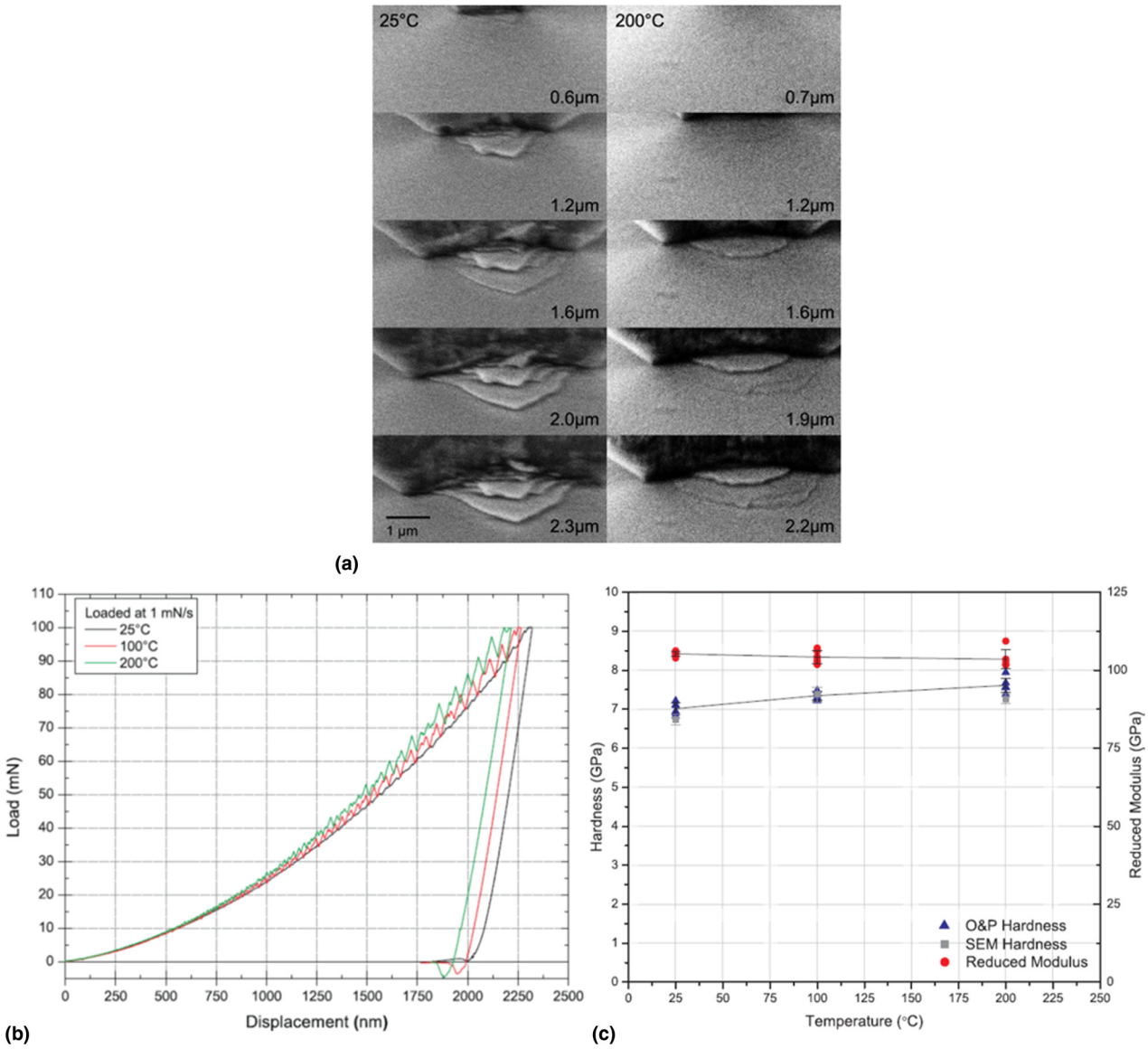

Figure 6. (a) In-situ scanning electron microscopy (SEM) pile-up deformation of a Zr-based BMG at 25 °C and 200 °C, (b) *P-h* curves for indentations loaded at 1 mN/s at different temperatures, (c) Hardness and reduced modulus as a function of temperature. Adopted with permission from Ref.[45] (Elsevier, 2011).

conductivity of Si under high-pressure loading, explained by a semiconductor–metal phase transition. Under room temperature condition, Si transforms to a metallic phase with β-Sn (Si-II) structure at a pressure of ~11–13 GPa, and further phase transforms (depending on unloading conditions) to amorphous silicon (*a*-Si) and/or the high-pressure crystalline phases Si-III (bc8, body-centered cubic (BCC) structure), and Si-XII (r8, the rhombohedral distortion of bc8) on unloading, which shows semi-metallic electronic behaviors.[48–51] In-situ high-temperature nanoindentation studies uncover that the Si-II phase is unstable in a pristine Si matrix at high temperatures. The nucleation of Si-III and Si-XII phases during unloading is intensified with the increase of temperature, however, the final phases depend on their thermal stability.

As shown in Fig. 7, an unusual "bowing" occurs on the *P-h* curve at 200 °C, which is attributed to the direct Si-II to Si-I transformation accompanied by rapid volume expansion. In fact, "bowing" phenomenon is detected for temperatures above ~125 °C. Furthermore, due to the rapid volume expansion as a result of the abrupt formation of Si-III/Si-XII during unloading of relaxed *a*-Si (relaxed by annealing), a pop-out event happens. However, no pop-out occurs for the unrelaxed *a*-Si.[52,53] Kiran et al.[54] showed that relaxed *a*-Si undergoes a pressure-induced phase transformation, either crystalline (Si-III/Si-XII) end phases or pressure-induced *a*-Si, at temperatures below 100 °C, as illustrated in Fig. 8.

However, at higher temperatures, plastic flow dominates the mode of deformation. It can be postulated that synergy of

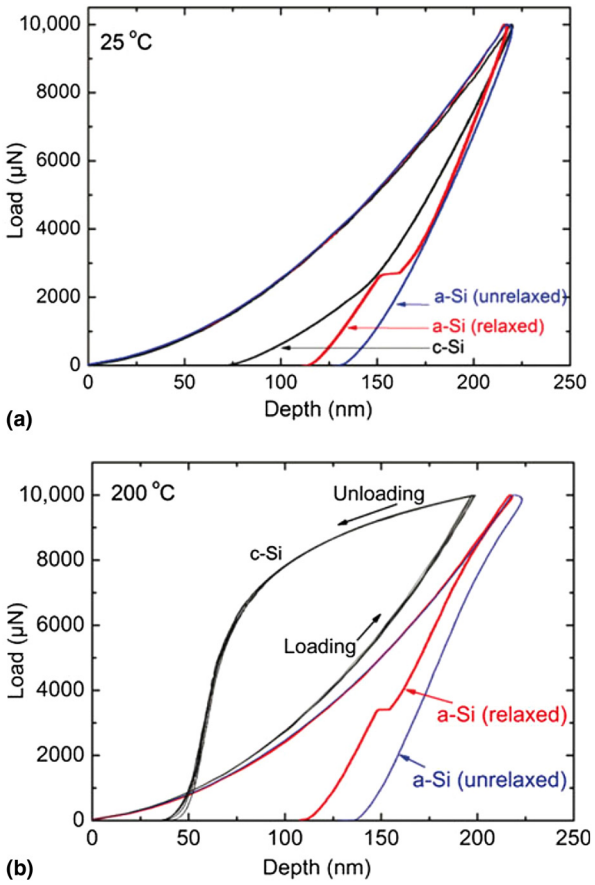

Figure 7. *P-h* curves of pristine Si (c-Si), relaxed and unrelaxed *a*-Si at (a) 25 °C and (b) 200 °C. Unusual "bowing" behavior of pristine Si at 200 °C is observable. Relaxed *a*-Si shows a "pop-out" event. Adopted with permission from Ref.[52] (Cambridge University Press, 2012).

pressure and temperature can cause bond softening and defect formation in relaxed *a*-Si, resulting in the inhibition of phase transformation owing to pressure-releasing plastic flow beneath the indenter. Interestingly, unrelaxed *a*-Si does not undergo phase transformation; rather it deforms completely via plastic flow up to 200 °C.[54] Si-VIII phase has also been observed during unloading at 100–125 °C,[55] whereas at temperatures above 350 °C, no phase transformation has been reported.[56]

Figure 9 presents the cross-sectional TEM (XTEM) bright and dark-field images of residual Berkovich indents of Si at different temperatures, along with selected area diffraction (SAD) patterns from the regions directly underneath the residual indents. Indents made at 25 and 100 °C, Figs. 9(a) and 9(b), show the presence of phase transformed zones within the deformed volume. Apart from Si reflections, there are several extra diffraction spots which are known to be characteristic reflections from polycrystalline Si-III and/or Si-XII phases. At 150 and 200 °C, only a very small phase transformed volume can be noticed. However, twinning along {111} planes is dominant at these temperatures, as illustrated in Figs. 9(c) and 9(d). Figure 10 depicts the deformation processes in Si under a nanoscale Berkovich indenter in the temperature range 25–200 °C, signifying that both phase transformation and defect propagation occur but to different extents depending on the indentation temperature.[57]

It is worthwhile to note that due to its technological importance, Si has remained an interesting material for high-temperature deformation mechanism studies and it is expected that, by using novel in-situ observation techniques, further issues will be uncovered in the following years. On the other hand, although Si and Ge are well-characterized materials in semiconductor section, other semiconductors, such as lithium niobate ($LiNbO_3$ or LN), have not been explored as systematically. LN is also called the "silicon of photonics", and is indispensable in advanced photonics and nonlinear optics. Furthermore, since these semiconductors should be cut and polished to produce a qualified wafer, they undergo several mechanical treatments which are directly associated with their deformation behavior at higher temperatures. These issues certainly point to the need for further research specifically addressing the role of temperature on the fundamental mechanical deformation of such semiconductor materials.

TEM images in Fig. 11 demonstrate that at room temperature, the transformed region in Ge comprises a BCC structure and the original diamond structure, whereas at 400 °C twinning in the diamond structure mainly drives the deformation. SAD analysis also reveals the presence of hexagonal structure at high temperatures,[58] both at the intersection of twins and in ribbons by the passage of a secondary twin,[59] indicating that the pressure-induced phase transformation to the β-Sn structure occurs at 400 °C. This observation is in line with the fact that hardness (4 ± 1 GPa) is lower than the pressure required to induce the phase transformation (~7–10 GPa, depending on the presence of shear stresses.[60])

Analysis of the high-temperature nanoindentation of shape memory alloy (SMA) Ni-Ti at 110 °C confirms that the martensite phase is converted to austenite at high temperatures, which demonstrates the mechanical properties akin to the austenite at room temperature, underscoring the thermally-induced phase transformations of Ni-Ti. Besides, the Young's modulus and hardness of the martensite films are smaller than those of the austenite films.[61] Pseudoelasticity (also referred to as superelasticity) of SMAs is usually linked with the reversible austenite-martensite phase transformation characterized by diffusionless, shear-induced atomic rearrangement. The occurrence of pseudoelasticity of martensitic Ni-Ti films is possible at the nanoscale over a specific temperature range without the evolution of martensite-austenite transformation. At an intermediate temperature of 55 °C, the anomalous pseudoelastic behavior of martensitic Ni-Ti films driven by increased twinned structure mobility can be realized.[62] The deformation mechanisms and the energy dissipated in the martensitic Ni-Ti films which exhibit pseudoelasticity are usually interpreted in terms of the behavior of metastable pseudotwins in the stress-induced martensite.[62,63]

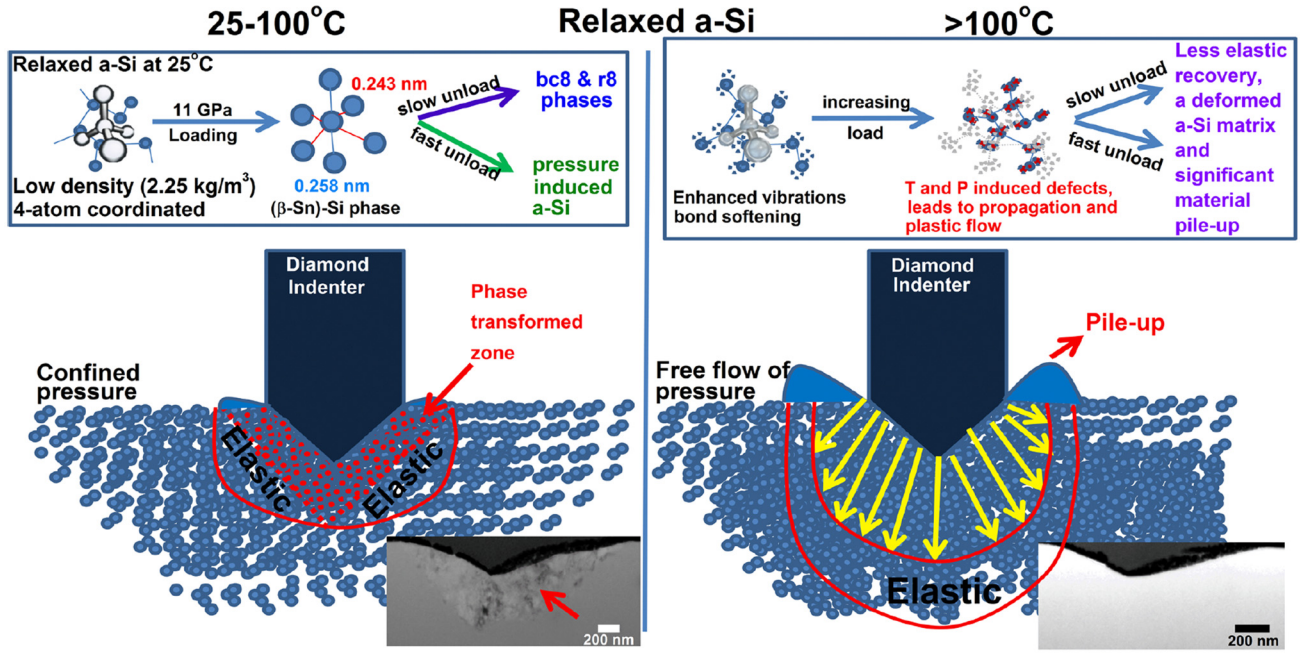

Figure 8. Deformation of relaxed *a*-Si at different temperatures. Adopted with permission from Ref.[54] (American Institute of Physics, 2014).

Mechanical properties

High-temperature nanoindentation can be used for measuring mechanical properties of materials, mainly hardness and elastic modulus, at elevated temperatures. For high-temperature nanoindentation and/or viscoelastic-plastic materials, e.g., polymeric materials, where the deformation is time-dependent and pile-up or sink-in is significant around the contact impression, the modified Oliver-Pharr method has to be adopted, where the true (elastic) contact stiffness, S_e, is used:[64,65]

$$\frac{1}{S_e} = \frac{1}{S} + \frac{\dot{h}_h^{\alpha}}{|\dot{P}|} \tag{1}$$

$$E_r = \frac{\sqrt{\pi}}{2\beta}\frac{S_e}{\sqrt{A}} \tag{2}$$

$$\frac{1}{E_r} = \frac{1-\nu^2}{E} + \frac{1-\nu_i^2}{E_i} \tag{3}$$

$$H = \frac{P}{A} \tag{4}$$

where $\dot{h}_h$ is the indenter displacement rate at the onset of unloading, $|\dot{P}|$ is the unloading rate, α is a positive dimensionless constant exponent, β is the correction factor for the indenter shape ($\beta = 1.034$–1.09 for a Berkovich indenter), E_r is the reduced modulus, A is the contact area, E, ν and E_i, ν_i stand for the elastic Young's modulus and Poisson's ratio of the sample and indenter, respectively. The hardness of the sample is calculated from Eq. 4.

Another recently-developed technique is to calculate a correction factor for the contact area calculated using the surface acoustic wave (SAW)[66] measurement which allows a correct hardness value, accounting for the pileup, to be determined.[67] This is a new and interesting approach for determining the true hardness and modulus which is expected to be pursued further in the coming years. An alternative method is the direct imaging of the residual impression[68] to determine the projected area. Such direct imaging technique is suitable for the cases where the edges of the residual indent impression (phase transformed or plastically deformed zone) are clearly visible owing to changes in surface morphology. In other words, the measurement of the indentation hardness by direct imaging is only correct if the measurement of the projected area captures the full phase transformed or plastically deformed area during loading.[69]

Notice open questions regarding the oxide film/substrate system still remain, particularly for high-temperature nanoindentation experiments. Although a preparatory explanation for the effect of the oxide film on the mechanical properties of a substrate was proposed by Tsui and Pharr,[70] further experimental and theoretical work are required to pinpoint the impact of oxide film/substrate system on the measured modulus and to propose new schemes to eliminate it from the measurements.

While the detailed literature on the determination of mechanical properties using high-temperature nanoindentation is extensive, most work identically reported the deterioration of mechanical properties with increasing temperature. Figure 12 illustrates the temperature versus percentage of hardness/

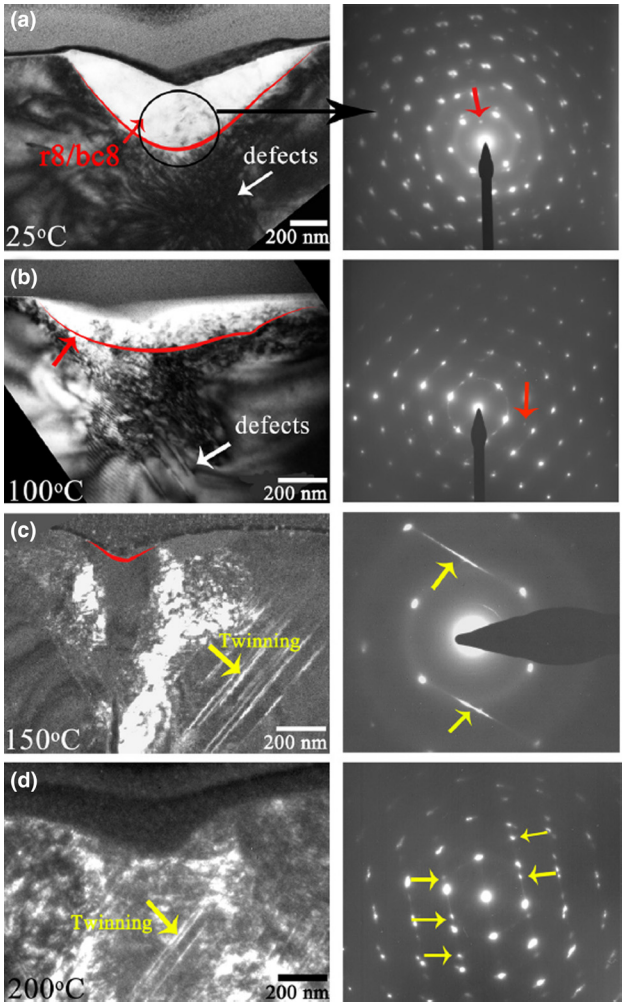

Figure 9. (a) and (b) Bright-field and (c) and (d) Dark-field XTEM images along with the SAD patterns of Berkovich indents indented on Si. Diffraction spots from bc8/r8 are pointed to by red arrows. The yellow arrows in (c) and (d) represent twinning and in their corresponding SAD patterns represent streaking and spot splitting due to twinning, respectively. For clarity, the red lines in (a), (b), and (c) illustrate the boundary between phase transformed and untransformed volumes under the indenter. Adopted with permission from Ref.[57] (American Institute of Physics, 2015).

Young's modulus reduction with respect to the room temperature values for different materials. Clearly, hardness is more affected by the temperature than Young's modulus. In support to Fig. 12, some interesting findings on the indentation response of materials at high temperatures are summarized in Table 1. It is instructive to note that the effect of nanoindentation speed (loading rate) on the resulting mechanical properties of materials is less pronounced at high temperatures. For example, as seen in Fig. 13, indentation hardness of high-purity Cr becomes strain-rate independent at a high temperature of 400 °C.[32] Less pronounced ISE at high temperatures has also been observed for Fe-Cr-Ni alloy 800H, which is attributed to the larger plastic zone size or the storage volume of geometrically necessary dislocations (GNDs).[82]

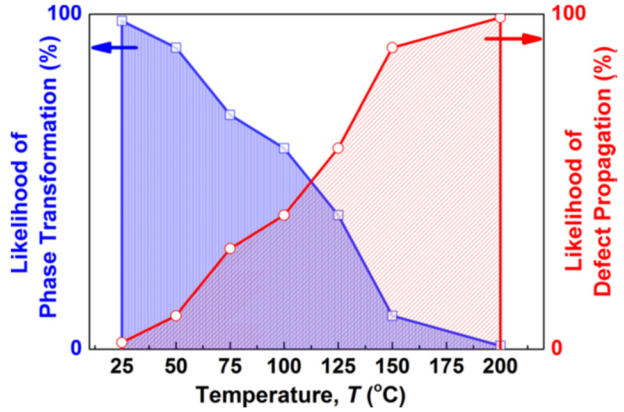

Figure 10. Schematic of the temperature dependence of the deformation mechanisms of diamond cubic Si under a nanoscale Berkovich indenter. Adopted with permission from Ref.[57] (American Institute of Physics, 2015).

As a final note, we remark that the location where the indenter is applied, e.g., GB or grain interior, can affect the nanoindentation response of the nano/polycrystalline materials. The same goes for the multi-phase materials, where various grains belonging to the same phase could have different grain size, elemental distribution, and grain orientation. For instance, room temperature indentation studies of a multi-phase quench and partitioning (Q&P) steel indicate that indentation hardness generally decreases with increasing distance from the GB in tempered martensite, which is attributed to the higher GNDs density near the GB, GB strengthening or carbon diffusion from martensite to retained austenite during the partitioning process.[102] On the other hand, the grains of the ferrite phase in a dual phase steel are found to be harder in the vicinity of martensitic grains.[103] Higher values of indentation hardness of austenitic phase compared to ferritic in transformation-induced plasticity steels, and specific pop-in events resulting from the onset of strain-induced martensitic transformation has also been reported,[104,105] which contradicts the hardness values obtained from the austenitic-ferritic duplex stainless steel, where the ferrite is the harder phase.[106] These room temperature studies point to the fact that one should be careful while measuring nanomechanical properties of multi-phase materials using nanoindentation instrument at low and high temperatures. It may also be noted that in spite of relatively detailed knowledge about the room temperature nanoindentation of multiphase steels, the temperature-dependent indentation behavior and high-temperature phase transformation of martensite, austenite, and ferrite in multiphase steels remains unexplored. This is an exciting area of further research which is encouraged for future work.

Remarks and perspective

Engineering materials exhibit temperature dependency in their physical and mechanical properties, arising from activities of

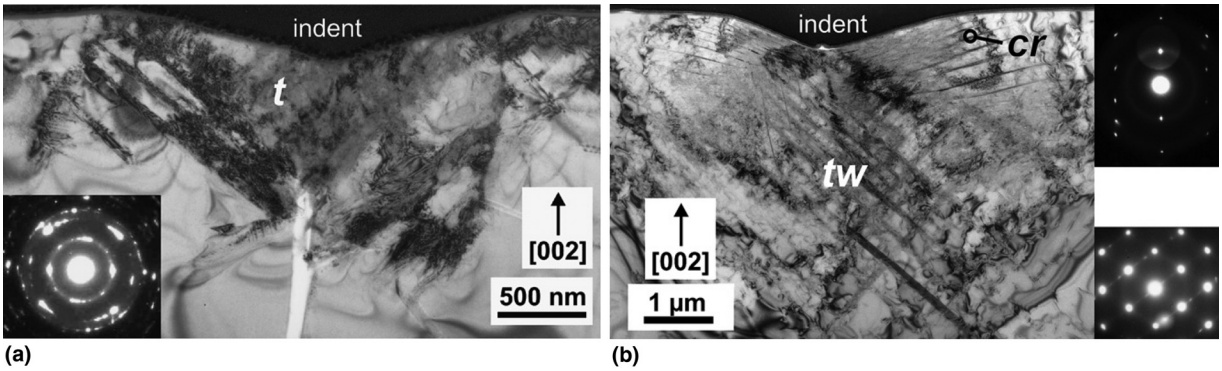

Figure 11. TEM bright-field image demonstrating (a) Phase transformation in Ge, marked '*t*', at room temperature, (b) Hexagonal crystal structure ('cr') and twinning ('tw') at 400 °C. Adopted with permission from Ref.[58] (Elsevier, 2007).

phonons (crystalline insulators and some semi-conductors), electrons (metal and some semi-conductors), propagons, diffusons, and locons (amorphous non-metallic materials), as well as thermal activation and phase transformation processes. A fundamental understanding of the temperature effects on the nanomechanical behavior and corresponding underlying mechanisms of nanostructured materials in the temperature regime of interest is critical for designing and developing micro/nanoelectromechanical systems, where surface atoms in contact regions are subjected to certain forms of loading at service temperatures. High-temperature nanoindentation renders a novel approach to uncover the nanomechanical behavior at elevated temperatures as well as thermally-activated processes and incipient plasticity in materials. In particular, recent breakthrough in in-situ high-temperature nanoindentation measurements, e.g., in-situ SEM,[7,45,107] in-situ Raman, in-situ TEM techniques, allow the real-time study of the interplay between mechanical, thermal, and electrical effects at the nanoscale. In general, the ability to implement multiple measurements simultaneously and to combine information from multiple analyses and techniques is highly desirable for nanoscale material characterization at high temperatures. As a result of the great capability of the in-situ measurements, it is envisioned that this arena will be pursued further by researchers in the upcoming years. Such technical advances in in-situ high-temperature nanoindentation instrumentation and their capabilities can benefit other in-situ thermomechanical testing methods such as high-temperature microcompression, as identical equipment can be used for characterization of multi-functionality at the nanoscale.

In addition, knowledge of the true contact area is very important for the successful determination of indentation

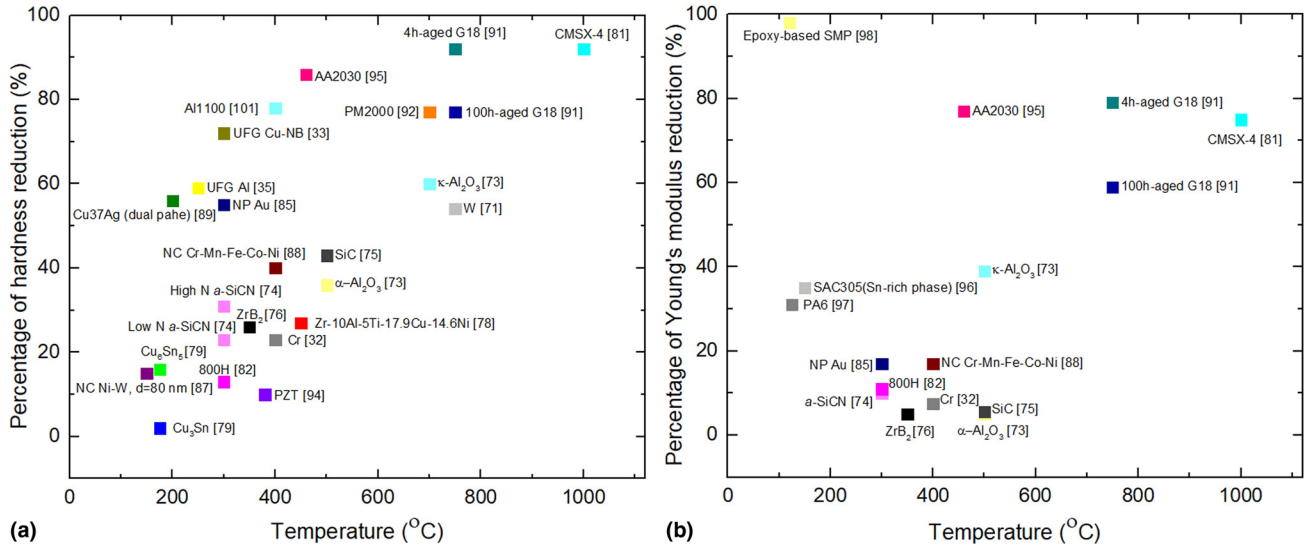

Figure 12. Percentage of (a) hardness (b) Young's modulus reduction as a function of temperature. The percentage values are calculated with respect to their values at room temperature. For further information, see Table 1.

Table I. Overview of nanoindentation mechanical responses of different materials at high temperatures.

Material	Primary characteristics of mechanical responses
W	Decrease of hardness up to 54% at 150 °C;[71] Increase of creep and creep recovery with temperature.[72]
Cr	Discontinuity of elastic modulus at the magnetic phase transition from antiferromagnetic order to the paramagnetic phase at 35 °C.[32]
α-Al_2O_3	Significant decrease of hardness (~36%) and a slight decrease of Young's modulus at 500 °C; Slight increase of Young's modulus and hardness at 600 °C due to oxidation of the substrate.[73]
κ-Al_2O_3	Constant hardness and Young's modulus up to 300 °C, followed by a decrease of hardness (up to 700 °C) and Young's modulus (up to 500 °C).[73]
a-SiCN	Drop of hardness up to 23% at 300 °C for *a*-SiCN with low nitrogen (N) content, and up to 31% for the *a*-SiCN with high N content; Increase of elastic modulus at 650 °C due to the pronounced effect of short-range ordering.[74]
SiC	Significant drop of hardness and slight decrease of elastic modulus up to 500 °C.[75]
ZrB_2	Increase of hardness at 450 °C and decrease at 600 °C; Erratic changes of elastic modulus at 400–600 °C, attributable to the increase from single to multiple slip plane systems, weakly $(10\bar{1}0)$ textured film and oxidation of the film or substrate.[76]
GaN	The higher the temperature, the lower the critical force for the pop-in in the *P-h* curve to occur.[77]
Zr-10Al-5Ti-17.9Cu-14.6Ni	Sudden drop in hardness above 400 °C caused by a structural relaxation at T_g.[78]
Cu_6Sn_5 and Cu_3Sn	Weak dependence of hardness and Young's modulus on temperature, and low creep rates up to 175 °C.[79,80]
CMSX-4	Constant hardness up to 400 °C followed by considerable softening, 92%, at 1000 °C.[81]
Fe-Cr-Ni alloy 800H	Decrease of hardness with increasing temperature, whereas reduced modulus remains relatively constant.[82]
Ni-Ti	More strain recovery at higher temperatures.[83]
UFG Al	Significantly higher hardness than CG Al at room temperature, but converges towards the CG Al hardness at higher temperatures; Absence of pile-up at temperatures ≥200 °C.[35]
UFG Cr	Increase of strain-rate sensitivity (SRS) above the critical temperature 150–225 °C caused by thermally-activated dislocation-GB interactions in the UFG state with the grain size of 300 nm, as opposed to the constant decrease of SRS for single crystal Cr with increasing temperature.[84]
UFG Cu-Nb	Increase of SRS up to 400 °C, followed by a drop at 500 °C, owing to a coarsened microstructure.[33]
Nanoporous (NP) Au	Increase of hardness up to 100 °C, then decrease up to 300 °C, explained by the substantial reduction of mobile dislocations upon annealing of the foam, as dislocations are able to exit at free surfaces.[85]
Ultra-fine porous Cu	Increase of hardness and Young's modulus with temperature, due to oxidation of the top of the ligaments which hinders dislocations to exit from the surface and dislocations are piled-up at the oxide–metal interface.[86]
Nanocrystalline (NC) Ni-W	Less pronounced thermal softening at finer grain sizes, e.g., 3 nm.[87]
NC Cr-Mn-Fe-Co-Ni alloy	Increase of SRS and constant activation volume above 100–150 °C, attributed to deformation governed by thermally-activated interactions between dislocations with high angle GBs.[88]
NC Cu37Ag	More pronounced decrease of hardness in the dual-phase regions at high temperatures than in the single-phase regions, suggesting that a temperature rise does not cause a softening in the shear bands compared to the nearby matrix.[89]
Cellulose nanocrystal	Increase of hardness and modulus at 150 °C due to decomposition of cellulose nanocrystal films from switchgrass.[90]
Multi-phase glass-ceramic G18	A slight increase of hardness before T_g in 100 h-aged sample; More pronounced decrease of hardness in 4 h-aged sample compared to100 h-aged sample due to the higher amount of glassy phase in the lesser-aged sample.[91]
Fe-based alumina-forming alloy PM2000	Dominance of creep for temperatures above 500 °C, correlated with a strongly decreasing stress exponent with increasing temperature.[92]

Nb-based alloy	Relatively stable elastic modulus and hardness up to 400 °C, followed by an increase due to the oxidation effects.[93]
PZT	Increase of indentation depth and modulus with temperature owing to the reduction of recoverable indentation depth induced by back-switched domains.[94]
AA2030	Decrease of hardness and Young's modulus, and increase of SRS and activation volume with increasing temperature.[95]
SAC305	Independence of Young's modulus of the eutectic phase to temperature; Larger creep deformation of the Sn-rich phase than that of eutectic phase; Greater SRS of eutectic phase at the temperature regime of 25–130 °C attributable to the mismatch between the β-Sn and intermetallic compound components in the eutectic microstructure.[96]
PA6	No close correlation between the tensile and nanoindentation modulus at high temperatures, attributable to the shift in the T_g of PA6 owing to the hydrostatic stress imposed by the indenter.[97]
Epoxy-based shape memory polymer (SMP)	Indent recovery is small in the glassy state (60–75 °C) and then increases in the transition state (93–98 °C), for which T_g = 105 °C.[98]
PMMA	Change of Young's modulus by a factor of 10^3 at T_g = 111.2 °C, whereas indentation and remanence depth changes only about a factor of 2–3.[99]
PtBA	Decrease of contact stiffness with increasing temperature; $T_g \approx 35.5 \pm 1.0$ °C obtained by a new technique modulated nanoindentation, which can be adopted for thermal transition analysis of polymer thin films.[100]
Al1100	A significant drop about 78% in hardness at a high temperature of 400 °C; an excellent fit of indentation creep data to the Garofalo type hyperbolic sine function at high temperatures.[101]

hardness and modulus. One paramount consideration when determining the mechanical properties of materials is that, although conventional methods such as the Oliver-Pharr[108] and Field-Swain[109] approximations for estimating contact depth are robust and directly applicable to room temperature nanoindentation and elastic-plastic materials, measurements of the contact depth for high temperature nanoindentation and/or viscoelastic-plastic materials, where deformation is time-dependent and pile-up or sink-in is significant around the contact impression, ought to be conducted using modified schemes such as the modified Oliver-Pharr method[65] to avoid any over-estimation of the reduced modulus and hardness. New methods and measurement techniques such as SAW[67] and direct imaging of the residual impression[68] can also be adopted to tackle this challenging problem. Such issues remain unsolved for most commercial nanoindentation instruments. It is therefore anticipated that determination of the true hardness and modulus will be advanced further in the near future.

Finally, we remark that with further advancements in computational modeling techniques, it will be feasible to gain clear insights into the temperature-dependent nanoindentation behavior and thermally-activated processes in functional materials. Particularly, a combination of the atomistic-based modeling and in-situ nanoindentation experiments provides a promising means to address the defect formation processes in crystalline and non-crystalline materials.

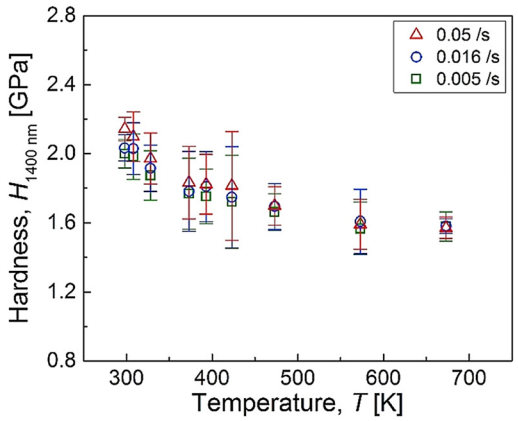

Figure 13. Indentation hardness of high-purity Cr as a function of temperature and strain-rate. Adopted with permission from Ref.[32] (Elsevier, 2017).

Acknowledgment

SZC would like to express his sincere gratitude for the financial support from the BIAM-Imperial Centre for Materials Characterization, Processing, and Modeling at Imperial College London. The work of SX was supported in part by the Elings Prize Fellowship in Science offered by the California NanoSystems Institute (CNSI) on the UC Santa Barbara campus.

References

1. W.K. Liu, E.G. Karpov, and H.S. Park: *Nano mechanics and materials: theory, multiscale methods and applications* (John Wiley & Sons, England, 2006).
2. B.D. Beake and J.F. Smith: High-temperature nanoindentation testing of fused silica and other materials. *Philos. Mag. A* **82**, 2179–2186 (2002).
3. J. Wheeler, D. Armstrong, W. Heinz, and R. Schwaiger: High temperature nanoindentation: the state of the art and future challenges. *Current Opinion Solid State Mater. Sci.* **19**, 354–366 (2015).

4. W. Kang, M. Merrill, and J.M. Wheeler: In situ thermomechanical testing methods for micro/nano-scale materials. *Nanoscale* **9**, 2666–2688 (2017).
5. J.C. Trenkle, C.E. Packard, and C.A. Schuh: Hot nanoindentation in inert environments. *Rev. Sci. Instrum.* **81**, 073901–073914 (2010).
6. J. Wheeler, P. Brodard, and J. Michler: Elevated temperature, in situ indentation with calibrated contact temperatures. *Philos. Mag.* **92**, 3128–3141 (2012).
7. J. Wheeler and J. Michler: Elevated temperature, nano-mechanical testing in situ in the scanning electron microscope. *Rev. Sci. Instrum.* **84**, 045103–045118 (2013).
8. C.A. Schuh, C.E. Packard, and A.C. Lund: Nanoindentation and contact-mode imaging at high temperatures. *J. Mater. Res.* **21**, 725–736 (2006).
9. C.E. Packard, J.M. Wheeler, J.C. Trenkle, and C.A. Schuh: Nanoindentation: high temperature. In *Reference Module in Materials Science and Materials Engineering* (Elsevier, 2016).
10. C. Schuh, J. Mason, A. Lund, and A. Hodge. *High temperature nanoindentation for the study of flow defects*. in MRS Proceedings (Cambridge University Press, 2004).
11. M.C. Wingert, J. Zheng, S. Kwon, and R. Chen: Thermal transport in amorphous materials: a review. *Semicond. Sci. Technol.* **31**, 113003 (2016).
12. P.E. Hopkins, M. Ding, and J. Poon: Contributions of electron and phonon transport to the thermal conductivity of GdFeCo and TbFeCo amorphous rare-earth transition-metal alloys. *J. Appl. Phys.* **111**, 103533 (2012).
13. S.Z. Chavoshi, S. Goel, and X. Luo: Molecular dynamics simulation investigation on the plastic flow behaviour of silicon during nanometric cutting. *Model. Simul. Mater. Sci. Eng.* **24**, 015002 (2015).
14. S.Z. Chavoshi, S. Goel, and X. Luo: Influence of temperature on the anisotropic cutting behaviour of single crystal silicon: a molecular dynamics simulation investigation. *J. Manuf. Process.* **23**, 201–210 (2016).
15. S.Z. Chavoshi and X. Luo: An atomistic simulation investigation on chip related phenomena in nanometric cutting of single crystal silicon at elevated temperatures. *Comput. Mater. Sci.* **113**, 1–10 (2016).
16. S.Z. Chavoshi and X. Luo: Atomic-scale characterization of occurring phenomena during hot nanometric cutting of single crystal 3C-SiC. *RSC Adv.* **6**, 71409–71424 (2016).
17. S.Z. Chavoshi, S. Xu, and X. Luo: Dislocation-mediated plasticity in silicon during nanometric cutting: a molecular dynamics simulation study. *Mater. Sci. Semicond. Process.* **51**, 60–70 (2016).
18. S.Z. Chavoshi and X. Luo: Molecular dynamics simulation study of deformation mechanisms in 3C–SiC during nanometric cutting at elevated temperatures. *Mater. Sci. Eng.: A* **654**, 400–417 (2016).
19. H. Mathur, V. Maier-Kiener, and S. Korte-Kerzel: Deformation in the γ-Mg 17 Al 12 phase at 25–278° C. *Acta Mater.* **113**, 221–229 (2016).
20. L. Shen, Y. Wu, S. Wang, and Z. Chen: Creep behavior of Sn–Bi solder alloys at elevated temperatures studied by nanoindentation. *J. Mater. Sci., Mater. Electron.* **28**, 4114–4124 (2017).
21. X. Kong, X. Kong, F. Sun, F. Sun, M. Yang, M. Yang, Y. Liu, and Y. Liu: High temperature creep properties of low-Ag Cu/Sn-Ag-Cu-Bi-Ni/Cu solder joints by nanoindentation method. *Solder. Surf. Mount Technol.* **28**, 167–174 (2016).
22. K. Rajulapati, M. Biener, J. Biener, and A. Hodge: Temperature dependence of the plastic flow behavior of tantalum. *Philos. Mag. Lett.* **90**, 35–42 (2010).
23. O. Franke, J. Alcalá, R. Dalmau, Z.C. Duan, J. Biener, M. Biener, and A. M. Hodge: Incipient plasticity of single-crystal tantalum as a function of temperature and orientation. *Philos. Mag.* **95**, 1866–1877 (2015).
24. G.I. Taylor: The mechanism of plastic deformation of crystals. Part I. Theoretical. Proceedings of the Royal Society of London. *Ser. A, Containing Papers Math. Phys. Character* **145**, 362–387 (1934).
25. K. Durst, B. Backes, O. Franke, and M. Göken: Indentation size effect in metallic materials: modeling strength from pop-in to macroscopic hardness using geometrically necessary dislocations. *Acta Mater.* **54**, 2547–2555 (2006).
26. W.D. Nix and H. Gao: Indentation size effects in crystalline materials: a law for strain gradient plasticity. *J. Mech. Phys. Solids* **46**, 411–425 (1998).
27. X. Qiu, Y. Huang, W. Nix, K. Hwang, and H. Gao: Effect of intrinsic lattice resistance in strain gradient plasticity. *Acta Mater.* **49**, 3949–3958 (2001).
28. A.C. Lund, A.M. Hodge, and C.A. Schuh: Incipient plasticity during nanoindentation at elevated temperatures. *Appl. Phys. Lett.* **85**, 1362–1364 (2004).
29. C. Schuh, J. Mason, and A. Lund: Quantitative insight into dislocation nucleation from high-temperature nanoindentation experiments. *Nat. Mater.* **4**, 617–621 (2005).
30. J. Mason, A. Lund, and C. Schuh: Determining the activation energy and volume for the onset of plasticity during nanoindentation. *Phys. Rev. B* **73**, 054102 (2006).
31. M. Haghshenas, V. Bhakhri, R. Oviasuyi, and R. Klassen: Effect of temperature and strain rate on the mechanisms of indentation deformation of magnesium. *MRS Commun.* **5**, 513–518 (2015).
32. I.-C. Choi, C. Brandl, and R. Schwaiger: Thermally activated dislocation plasticity in body-centered cubic chromium studied by high-temperature nanoindentation. *Acta Mater.* **140**, 107–115 (2017).
33. M.-M. Primorac, M.D. Abad, P. Hosemann, M. Kreuzeder, V. Maier, and D. Kiener: Elevated temperature mechanical properties of novel ultra-fine grained Cu–Nb composites. *Mater. Sci. Eng.: A* **625**, 296–302 (2015).
34. V. Maier, K. Durst, J. Mueller, B. Backes, H.W. Höppel, and M. Göken: Nanoindentation strain-rate jump tests for determining the local strain-rate sensitivity in nanocrystalline Ni and ultrafine-grained Al. *J. Mater. Res.* **26**, 1421–1430 (2011).
35. J. Wheeler, V. Maier, K. Durst, M. Göken, and J. Michler: Activation parameters for deformation of ultrafine-grained aluminium as determined by indentation strain rate jumps at elevated temperature. *Mater. Sci. Eng.: A* **585**, 108–113 (2013).
36. N. Li, L. Liu, K. Chan, Q. Chen, and J. Pan: Deformation behavior and indentation size effect of Au 49 Ag 5.5 Pd 2.3 Cu 26.9 Si 16.3 bulk metallic glass at elevated temperatures. *Intermetallics* **17**, 227–230 (2009).
37. B. Yang, J. Wadsworth, and T.-G. Nieh: Thermal activation in Au-based bulk metallic glass characterized by high-temperature nanoindentation. *Appl. Phys. Lett.* **90**, 061911 (2007).
38. A. Argon: Plastic deformation in metallic glasses. *Acta Metall.* **27**, 47–58 (1979).
39. A. Argon and L.T. Shi: Development of visco-plastic deformation in metallic glasses. *Acta Metall.* **31**, 499–507 (1983).
40. R. Zallen: *The physics of amorphous solids* (John Wiley & Sons, Weinheim, 2008).
41. C.A. Schuh, A.C. Lund, and T. Nieh: New regime of homogeneous flow in the deformation map of metallic glasses: elevated temperature nanoindentation experiments and mechanistic modeling. *Acta Mater.* **52**, 5879–5891 (2004).
42. C.E. Packard, J. Schroers, and C.A. Schuh: In situ measurements of surface tension-driven shape recovery in a metallic glass. *Scr. Mater.* **60**, 1145–1148 (2009).
43. D.L. Henann and L. Anand: Surface tension-driven shape-recovery of micro/nanometer-scale surface features in a Pt 57.5 Ni 5.3 Cu 14.7 P 22.5 metallic glass in the supercooled liquid region: a numerical modeling capability. *J. Mech. Phys. Solids* **58**, 1947–1962 (2010).
44. G. Kumar and J. Schroers: Write and erase mechanisms for bulk metallic glass. *Appl. Phys. Lett.* **92**, 031901 (2008).
45. J. Wheeler, R. Raghavan, and J. Michler: In situ SEM indentation of a Zr-based bulk metallic glass at elevated temperatures. *Mater. Sci. Eng.: A* **528**, 8750–8756 (2011).
46. A. Bhattacharyya, G. Singh, K.E. Prasad, R. Narasimhan, and U. Ramamurty: On the strain rate sensitivity of plastic flow in metallic glasses. *Mater. Sci. Eng.: A* **625**, 245–251 (2015).
47. S. Minomura and H. Drickamer: Pressure induced phase transitions in silicon, germanium and some III–V compounds. *J. Phys. Chem. Solids* **23**, 451–456 (1962).
48. D. Ge, V. Domnich, and Y. Gogotsi: High-resolution transmission electron microscopy study of metastable silicon phases produced by nanoindentation. *J. Appl. Phys.* **93**, 2418–2423 (2003).
49. R. Piltz, J. Maclean, S. Clark, G. Ackland, P. Hatton, and J. Crain: Structure and properties of silicon XII: a complex tetrahedrally bonded phase. *Phys. Rev. B* **52**, 4072–4085 (1995).

50. S. Ruffell, J. Bradby, and J. Williams: High pressure crystalline phase formation during nanoindentation: amorphous versus crystalline silicon. *Appl. Phys. Lett.* **89**, 091919 (2006).
51. S.Z. Chavoshi, S.C. Gallo, H. Dong, and X. Luo: High temperature nanoscratching of single crystal silicon under reduced oxygen condition. *Mater. Sci. Eng.: A* **684**, 385–393 (2017).
52. S. Bhuyan, J. Bradby, S. Ruffell, B. Haberl, C. Saint, J. Williams, and P. Munroe: Phase stability of silicon during indentation at elevated temperature: evidence for a direct transformation from metallic Si-II to diamond cubic Si-I. *MRS Commun.* **2**, 9–12 (2012).
53. S. Ruffell, J. Bradby, J. Williams, D. Munoz-Paniagua, S. Tadayyon, L. Coatsworth, and P. Norton: Nanoindentation-induced phase transformations in silicon at elevated temperatures. *Nanotechnology* **20**, 135603–135608 (2009).
54. M. Kiran, B. Haberl, J. Williams, and J. Bradby: Temperature dependent deformation mechanisms in pure amorphous silicon. *J. Appl. Phys.* **115**, 113511 (2014).
55. R.K. Singh, P. Munroe, and M. Hoffman: Effect of temperature on metastable phases induced in silicon during nanoindentation. *J. Mater. Res.* **23**, 245–249 (2008).
56. V. Domnich, Y. Aratyn, W.M. Kriven, and Y. Gogotsi: Temperature dependence of silicon hardness: experimental evidence of phase transformations. *Rev. Adv. Mater. Sci.* **17**, 33–41 (2008).
57. M. Kiran, T. Tran, L. Smillie, B. Haberl, D. Subianto, J. Williams, and J. Bradby: Temperature-dependent mechanical deformation of silicon at the nanoscale: phase transformation versus defect propagation. *J. Appl. Phys.* **117**, 205901 (2015).
58. L. Vandeperre, F. Giuliani, S. Lloyd, and W. Clegg: The hardness of silicon and germanium. *Acta Mater.* **55**, 6307–6315 (2007).
59. S. Xiao and P. Pirouz: On diamond-hexagonal germanium. *J. Mater. Res.* **7**, 1406–1412 (1992).
60. C.S. Menoni, J.Z. Hu, and I.L. Spain: Germanium at high pressures. *Phys. Rev. B* **34**, 362 (1986).
61. X. Huang, J. Nohava, B. Zhang, and A. Ramirez: Nanoindentation of NiTi shape memory thin films at elevated temperatures. *Int. J. Smart Nano Mater.* **2**, 39–49 (2011).
62. X.-G. Ma and K. Komvopoulos: In situ transmission electron microscopy and nanoindentation studies of phase transformation and pseudoelasticity of shape-memory titanium-nickel films. *J. Mater. Res.* **20**, 1808–1813 (2005).
63. K. Komvopoulos and X.-G. Ma: Pseudoelasticity of martensitic titanium-nickel shape-memory films studied by in situ heating nanoindentation and transmission electron microscopy. *Appl. Phys. Lett.* **87**, 263108 (2005).
64. Y. Li, X. Fang, S. Lu, Q. Yu, G. Hou, and X. Feng: Effects of creep and oxidation on reduced modulus in high-temperature nanoindentation. *Mater. Sci. Eng.: A* **678**, 65–71 (2016).
65. G. Feng and A. Ngan: Effects of creep and thermal drift on modulus measurement using depth-sensing indentation. *J. Mater. Res.* **17**, 660–668 (2002).
66. J.A. Rogers, A.A. Maznev, M.J. Banet, and K.A. Nelson: Optical generation and characterization of acoustic waves in thin films: fundamentals and applications. *Annu. Rev. Mater. Sci.* **30**, 117–157 (2000).
67. C.E. Beck, F. Hofmann, J.K. Eliason, A.A. Maznev, K.A. Nelson, and D. E. Armstrong: Correcting for contact area changes in nanoindentation using surface acoustic waves. *Scr. Mater.* **128**, 83–86 (2017).
68. N. Fujisawa and M.V. Swain: On the indentation contact area of a creeping solid during constant-strain-rate loading by a sharp indenter. *J. Mater. Res.* **22**, 893–899 (2007).
69. B. Haberl, L.B.B. Aji, J. Williams, and J.E. Bradby: The indentation hardness of silicon measured by instrumented indentation: what does it mean? *J. Mater. Res.* **27**, 3066–3072 (2012).
70. T. Tsui and G. Pharr: Substrate effects on nanoindentation mechanical property measurement of soft films on hard substrates. *J. Mater. Res.* **14**, 292–301 (1999).
71. J.S.-L. Gibson, S.G. Roberts, and D.E. Armstrong: High temperature indentation of helium-implanted tungsten. *Mater. Sci. Eng.: A* **625**, 380–384 (2015).
72. A. Harris, B. Beake, D. Armstrong, and M. Davies: Development of high temperature nanoindentation methodology and its application in the nanoindentation of polycrystalline tungsten in vacuum to 950° C. *Exp. Mech.* **57**, 1115–1126 (2017).
73. M.R. de Figueiredo, M.D. Abad, A.J. Harris, C. Czettl, C. Mitterer, and P. Hosemann: Nanoindentation of chemical-vapor deposited Al 2 O 3 hard coatings at elevated temperatures. *Thin Solid Films* **578**, 20–24 (2015).
74. R. Ctvrtlik, M.S. Al-Haik, and V. Kulikovsky: Mechanical properties of amorphous silicon carbonitride thin films at elevated temperatures. *J. Mater. Sci.* **50**, 1553–1564 (2015).
75. N. Rohbeck, D. Tsivoulas, I.P. Shapiro, P. Xiao, S. Knol, J.-M. Escleine, and M. Perez: In-situ nanoindentation of irradiated silicon carbide in TRISO particle fuel up to 500° C. *J. Nucl. Mater.* **465**, 692–694 (2015).
76. E. Broitman, L. Tengdelius, U.D. Hangen, J. Lu, L. Hultman, and H. Högberg: High-temperature nanoindentation of epitaxial ZrB 2 thin films. *Scr. Mater.* **124**, 117–120 (2016).
77. J.-Y. Lu, H. Ren, D.-M. Deng, Y. Wang, K.J. Chen, K.-M. Lau, and T.-Y. Zhang: Thermally activated pop-in and indentation size effects in GaN films. *J. Phys. D: Appl. Phys.* **45**, 085301 (2012).
78. T. Nieh, C. Iwamoto, Y. Ikuhara, K. Lee, and Y. Chung: Comparative studies of crystallization of a bulk Zr–Al–Ti–Cu–Ni amorphous alloy. *Intermetallics* **12**, 1183–1189 (2004).
79. V. Marques, C. Johnston, and P. Grant: Nanomechanical characterization of Sn–Ag–Cu/Cu joints—Part 1: young's modulus, hardness and deformation mechanisms as a function of temperature. *Acta Mater.* **61**, 2460–2470 (2013).
80. V. Marques, B. Wunderle, C. Johnston, and P. Grant: Nanomechanical characterization of Sn–Ag–Cu/Cu joints—Part 2: Nanoindentation creep and its relationship with uniaxial creep as a function of temperature. *Acta Mater.* **61**, 2471–2480 (2013).
81. J.S.-L. Gibson, S. Schröders, C. Zehnder, and S. Korte-Kerzel: On extracting mechanical properties from nanoindentation at temperatures up to 1000° C. *Extreme Mech. Lett.* **17**, 43–49 (2017).
82. A. Prasitthipayong, S. Vachhani, S. Tumey, A. Minor, and P. Hosemann: Indentation size effect in unirradiated and ion-irradiated 800H steel at high temperatures. *Acta Mater.* **144**, 896–904 (2018).
83. A.M. Wood and T. Clyne: Measurement and modelling of the nanoindentation response of shape memory alloys. *Acta Mater.* **54**, 5607–5615 (2006).
84. V. Maier, A. Hohenwarter, R. Pippan, and D. Kiener: Thermally activated deformation processes in body-centered cubic Cr–How microstructure influences strain-rate sensitivity. *Scr. Mater.* **106**, 42–45 (2015).
85. A. Leitner, V. Maier-Kiener, J. Jeong, M. Abad, P. Hosemann, S. Oh, and D. Kiener: Interface dominated mechanical properties of ultra-fine grained and nanoporous Au at elevated temperatures. *Acta Mater.* **121**, 104–116 (2016).
86. M. Kreuzeder, M.-D. Abad, M.-M. Primorac, P. Hosemann, V. Maier, and D. Kiener: Fabrication and thermo-mechanical behavior of ultra-fine porous copper. *J. Mater. Sci.* **50**, 634–643 (2015).
87. J.R. Trelewicz and C.A. Schuh: Hot nanoindentation of nanocrystalline Ni–W alloys. *Scr. Mater.* **61**, 1056–1059 (2009).
88. V. Maier-Kiener, B. Schuh, E.P. George, H. Clemens, and A. Hohenwarter: Insights into the deformation behavior of the CrMnFeCoNi high-entropy alloy revealed by elevated temperature nanoindentation. *J. Mater. Res.* **32**, 2658–2667 (2017).
89. K. Kormout, P. Ghosh, V. Maier-Kiener, and R. Pippan: Deformation mechanisms during severe plastic deformation of a Cu Ag composite. *J. Alloys Compd.* **695**, 2285–2294 (2017).
90. Q. Wu, Y. Meng, K. Concha, S. Wang, Y. Li, L. Ma, and S. Fu: Influence of temperature and humidity on nano-mechanical properties of cellulose nanocrystal films made from switchgrass and cotton. *Ind. Crops Prod.* **48**, 28–35 (2013).
91. J. Milhans, D. Li, M. Khaleel, X. Sun, M.S. Al-Haik, A. Harris, and H. Garmestani: Mechanical properties of solid oxide fuel cell glass-ceramic seal at high temperatures. *J. Power Sources* **196**, 5599–5603 (2011).
92. U. Hangen, C.L. Chen, and A. Richter: Mechanical characterization of PM2000 oxide-dispersion-strengthened alloy by high temperature nanoindentation. *Adv. Eng. Mater.* **17**, 1683–1690 (2015).
93. Y. Li, X. Fang, B. Xia, and X. Feng: In situ measurement of oxidation evolution at elevated temperature by nanoindentation. *Scr. Mater.* **103**, 61–64 (2015).

94. Y. Li, S. Feng, W. Wu, and F. Li: Temperature dependent mechanical property of PZT film: an investigation by nanoindentation. *PLoS ONE* **10**, e0116478 (2015).
95. S. Koch, M.D. Abad, S. Renhart, H. Antrekowitsch, and P. Hosemann: A high temperature nanoindentation study of Al–Cu wrought alloy. *Mater. Sci. Eng.: A* **644**, 218–224 (2015).
96. F. Gao, H. Nishikawa, T. Takemoto, and J. Qu: Mechanical properties versus temperature relation of individual phases in Sn–3.0 Ag–0.5 Cu lead-free solder alloy. *Microelectron. Reliab.* **49**, 296–302 (2009).
97. R. Seltzer, J.K. Kim, and Y.W. Mai: Elevated temperature nanoindentation behaviour of polyamide 6. *Polym. Int.* **60**, 1753–1761 (2011).
98. J. Fulcher, Y. Lu, G. Tandon, and D. Foster: Thermomechanical characterization of shape memory polymers using high temperature nanoindentation. *Polym. Test.* **29**, 544–552 (2010).
99. M. Hinz, A. Kleiner, S. Hild, O. Marti, U. Dürig, B. Gotsmann, U. Drechsler, T. Albrecht, and P. Vettiger: Temperature dependent nano indentation of thin polymer films with the scanning force microscope. *Eur. Polym. J.* **40**, 957–964 (2004).
100. S. Sills, H. Fong, C. Buenviaje, M. Sarikaya, and R.M. Overney: Thermal transition measurements of polymer thin films by modulated nanoindentation. *J. Appl. Phys.* **98**, 014302 (2005).
101. P.S. Phani and W. Oliver: A direct comparison of high temperature nanoindentation creep and uniaxial creep measurements for commercial purity aluminum. *Acta Mater.* **111**, 31–38 (2016).
102. G. Cheng, K.S. Choi, X. Hu, and X. Sun: Determining individual phase properties in a multi-phase Q&P steel using multi-scale indentation tests. *Mater. Sci. Eng.: A* **652**, 384–395 (2016).
103. J. Kadkhodapour, S. Schmauder, D. Raabe, S. Ziaei-Rad, U. Weber, and M. Calcagnotto: Experimental and numerical study on geometrically necessary dislocations and non-homogeneous mechanical properties of the ferrite phase in dual phase steels. *Acta Mater.* **59**, 4387–4394 (2011).
104. T.-H. Ahn, C.-S. Oh, D. Kim, K. Oh, H. Bei, E.P. George, and H. Han: Investigation of strain-induced martensitic transformation in metastable austenite using nanoindentation. *Scr. Mater.* **63**, 540–543 (2010).
105. B. He, M. Huang, Z. Liang, A. Ngan, H. Luo, J. Shi, W. Cao, and H. Dong: Nanoindentation investigation on the mechanical stability of individual austenite grains in a medium-Mn transformation-induced plasticity steel. *Scr. Mater.* **69**, 215–218 (2013).
106. K.R. Gadelrab, G. Li, M. Chiesa, and T. Souier: Local characterization of austenite and ferrite phases in duplex stainless steel using MFM and nanoindentation. *J. Mater. Res.* **27**, 1573–1579 (2012).
107. J. Wheeler, C. Niederberger, C. Tessarek, S. Christiansen, and J. Michler: Extraction of plasticity parameters of GaN with high temperature, in situ micro-compression. *Int. J. Plast.* **40**, 140–151 (2013).
108. W.C. Oliver and G.M. Pharr: An improved technique for determining hardness and elastic modulus using load and displacement sensing indentation experiments. *J. Mater. Res.* **7**, 1564–1583 (1992).
109. J. Field and M. Swain: A simple predictive model for spherical indentation. *J. Mater. Res.* **8**, 297–306 (1993).